Characterizations of Basalt Unsaturated Polyester Laminates Under Static Three-Point Bending and Low-Velocity Impact Loadings

Rotich K. Gideon,[1] Hangjun Hu,[1] Paul Wambua,[2] Bohong Gu[1]
[1]*College of Textiles, Donghua University, Shanghai 201620, China*

[2]*School of Engineering, Moi University, 3900 Eldoret, Kenya*

This paper reports the responses of basalt unsaturated polyester laminates under static three-point bending loading and low-velocity impact. Three kinds of composite materials, unidirectional (0°), cross-ply (0°/90°) and woven laminates were considered. The laminates were fabricated by layup process and hot pressed under pressure. Static three-point bending tests and low-velocity impact tests were conducted to obtain the force–deflection, force–time, deflection–time, velocity–time, and energy–time curves. The results showed that unidirectional (0°) laminates carried more load during static loading, but in the event of dynamic loading, cross-ply, and woven laminates were more superior. It was observed that the failure of 0° laminates was along the fiber direction while for cross-ply and woven, the damage was localized, around the impacted locations. From the different combinations of unidirectional (0°), cross-ply (0°/90°) and woven lamina, the impact behaviors could be optimized with the lowest area density. POLYM. COMPOS., 35:2203–2213, 2014. © 2014 Society of Plastics Engineers

INTRODUCTION

Composite materials are increasingly being applied to high strength and low weight structures because of their advantage of higher stiffness, high strength to weight ratio, and the ability of being tailored for a specific use. The fibers currently used to reinforce composites face challenges [1]. Glass fiber, which is widely used, is susceptible to surface damage and loses its strength when exposed to alkaline conditions [2, 3]. Basalt fiber is produced from volcanic basalt rocks using either Junkers method which produces short fibers [4] or spinneret method which produces continuous fibers [5]. The advantage of basalt production method is that neither a precursor nor additives are required in the manufacturing route which is an economic gain [6]. Basalt fiber has a density of 2.6–2.7 g/cm^3, electrical properties 10 times better than glass and much better chemical resistance than glass fiber, especially, in strong alkalis [7, 8]. It can be used in a wider temperature range of −260°C to about 800°C [9]. Basalt fibers are used as reinforcement in composites in different ways: as short fibers reinforcement [4], as continuous fiber reinforcement and as an hybrid reinforcing fiber with other fibers [10–12].

A number of investigations have been done in comparing basalt fiber with other reinforcing fibers especially with glass fibers [2, 6, 7, 13]. The comparison of basalt fiber with glass fiber showed that they have better properties especially its chemical resistance in alkaline environment [2], higher Young's modulus, better compressive strength, and flexural behavior [6]. Colombo et al. [14] investigated static mechanical behaviors of basalt reinforced composites. It was found that BRC showed an overall lower trend in their mechanical properties but their utilization can be supported by their favorable ratio involving performances and costs. Tan et al. [15] investigated basalt fiber reinforced laminates (BFRL) subjected to elevated temperatures. They found that the basalt laminates exhibited smaller deterioration in ultimate strength when used at a higher temperature as compared to glass fiber laminates.

As for the low-velocity impact behaviors of basalt fiber-reinforced composite, Mathivanan et al. [16] found that the profound damage mode depends on the impactor parameters and the composites properties. The same conclusion was found by Aktas et al. [17] when they investigated the impact response of composite laminates. The results from their studies indicated that when a composite is subjected to a low-velocity impact event, it responds in three different ways: it can rebound the impactor, stop the impactor or the impactor can perforate the composite [16, 18, 19]. All these reactions depend on the energy possessed by the impactor and the composite properties [11]. Basalt fiber-

Correspondence to: Bohong Gu; e-mail: gubh@dhu.edu.cn
DOI 10.1002/pc.22885
Published online in Wiley Online Library (wileyonlinelibrary.com).

TABLE 1. Mechanical parameters of basalt fibers and unsaturated polyester resin.

	Tensile modulus (GPa)	Shear modulus (GPa)	Poisson's ratio	Tensile strength (MPa)	Compressive strength (MPa)	Shear strength (MPa)
Basalt fibers	90	0.34	0.23	4200	3500	1700
Unsaturated Polyester resin	6.8	2.46	0.38	48	143	74

reinforced laminates were expected to behave in the same way when subjected to low-velocity impact event.

The main aim of this work was to investigate the effect of different stacking sequence of basalt fiber reinforced laminate on the responses under static and low-velocity impact loadings. This work was also aimed at characterizing basalt-reinforced composite by three-point bending tests and low-velocity impact tests. Three stacking sequences, i.e., unidirectional reinforcement (0°), cross-ply reinforcement (0°/90°) and plain woven reinforcement were studied. We hope the investigations of the influences of stacking sequences on the low-velocity impact behaviors could be extended to the high impact damage-resistance laminate design.

EXPERIMENTAL

Materials

Basalt fibers and unsaturated polyester resin were used to manufacture basalt reinforced composite laminates. Basalt fiber was supplied by GBF® Company, Shanghai, China. The specific mass of the basalt fibers was 600tex (yarn measuring unit: 1 tex = 1000 m/g) with an average diameter of 7 μm. Unsaturated polyester resin was supplied by Swancor® Company, Shanghai, China. Unsaturated polyester was preferred because of its low cost, easiness in processability, and lower density. Curing agent and a catalyst were used to aid curing of the resin. The viscosity of the resin was 0.18 pas at 25°C and the curing agent was AKZO® M-50 mixed at a proportion of 100 parts of resin to 2 parts of curing agent by weight. Table 1 lists the mechanical parameters of basalt fibers and unsaturated polyester resin used and Fig. 1 shows stress–strain curves of the pure resin specimens under tensile, compressive, and shear loads.

Manufacturing of Samples

The basalt fibers were wound on to a board mould using a winding machine as shown in Fig. 2, ensuring that a uniform winding was achieved (the number of fibers per length was constant). Then resin mixed with the curing agent and a catalyst, was applied by use of an improvized blade as shown in Fig. 1. Precuring was done under a temperature of 60°C and pressure of 0.1 MPa, which led to the formation of a lamina. The lamina was released from the mould board by cutting the sides. The laminates were made through the layup process by stacking 12 layers together in the desired sequence and applying unsaturated polyester between them before curing in a hot press machine under a pressure of 6 MPa and temperature of 130°C for 3 h. The samples were cut with a high pressure water-jet cutter, into the required sample size as per the test to be carried out. The fiber mass fraction was 61.5% determined by burning test according to ASTM D 3171 standards.

Basalt plain fabric with a weaving density of 6 warps/cm and areal density of 600 g/m^2 was used. It was cut to the required size of 30 × 30 cm^2 and impregnated with resin using improvized blade after which they were precured with a temperature of 60°C and a pressure of 0.1 MPa. Six laminas were stack together to form a laminate by gluing with unsaturated polyester resin in between them and subjecting them to a temperature of 130°C and a pressure of 6 MPa to cure them for 3 h.

Tests

Static Three-Point Bending Test. Static three-point bending tests were conducted on an MTS® testing machine as shown in Fig. 3, according to ASTM D 7264 standards with a standard span-to-thickness ratio of 32:1. The specimen dimensions were 140 × 13 × 4 mm^3 while the span length was adjusted to 100 mm so as to diminish the effect of the through thickness shear deformation on the Young's modulus. Four types of samples having fiber orientation of 0°, 90°, 0°/90° and plain woven were tested. Five samples were tested for each type and the average was used. The machine loaded the specimen at

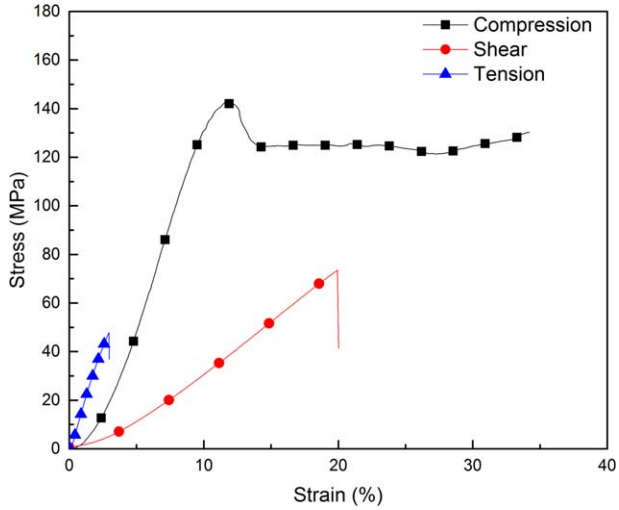

FIG. 1. Stress–strain curves of the pure resin specimens under tensile, compressive, and shear loads. [Color figure can be viewed in the online issue, which is available at wileyonlinelibrary.com.]

 DOI 10.1002/pc

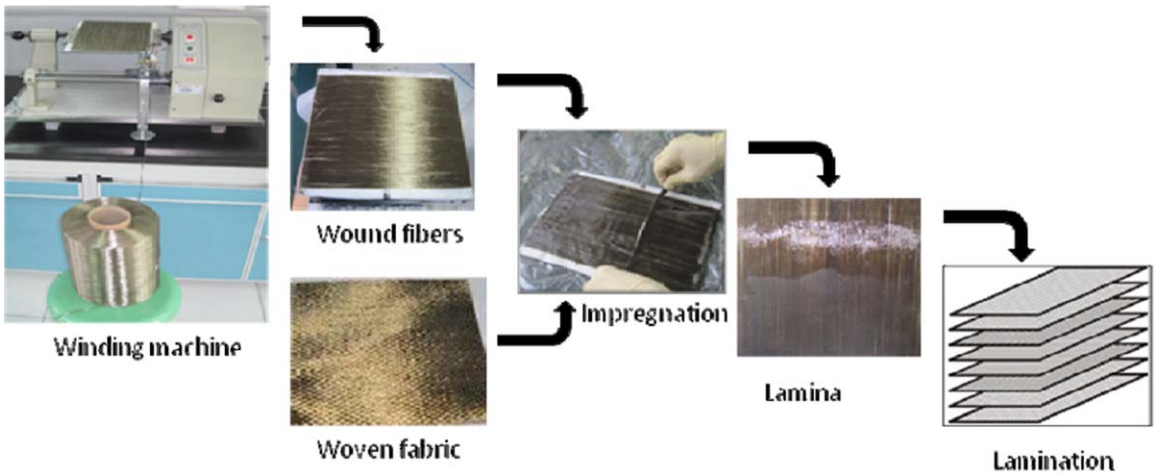

FIG. 2. Laminates manufacture. [Color figure can be viewed in the online issue, which is available at wileyonlinelibrary.com.]

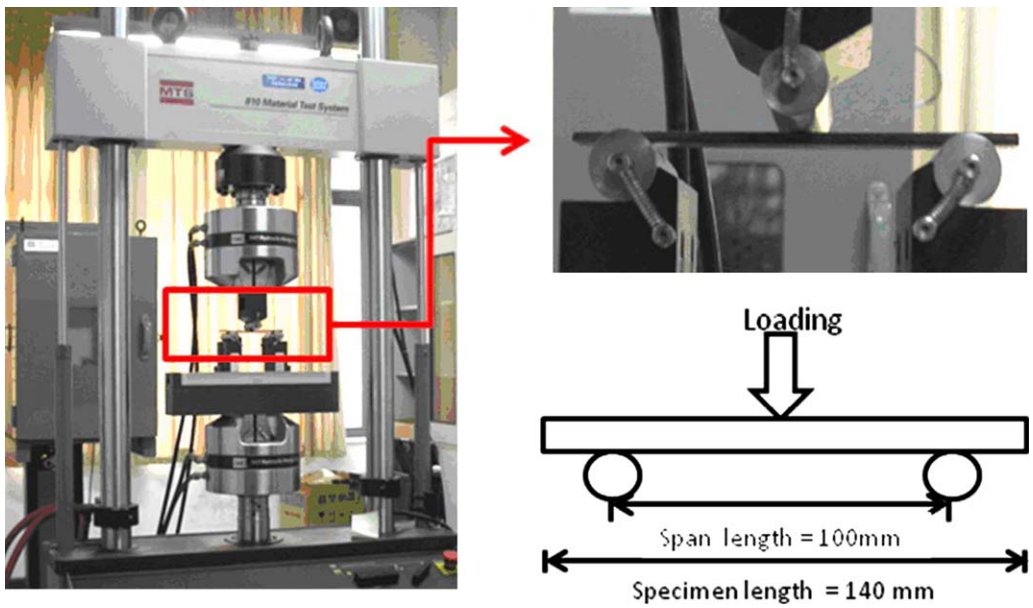

FIG. 3. MTS® testing machine for three-point static indentation tests. [Color figure can be viewed in the online issue, which is available at wileyonlinelibrary.com.]

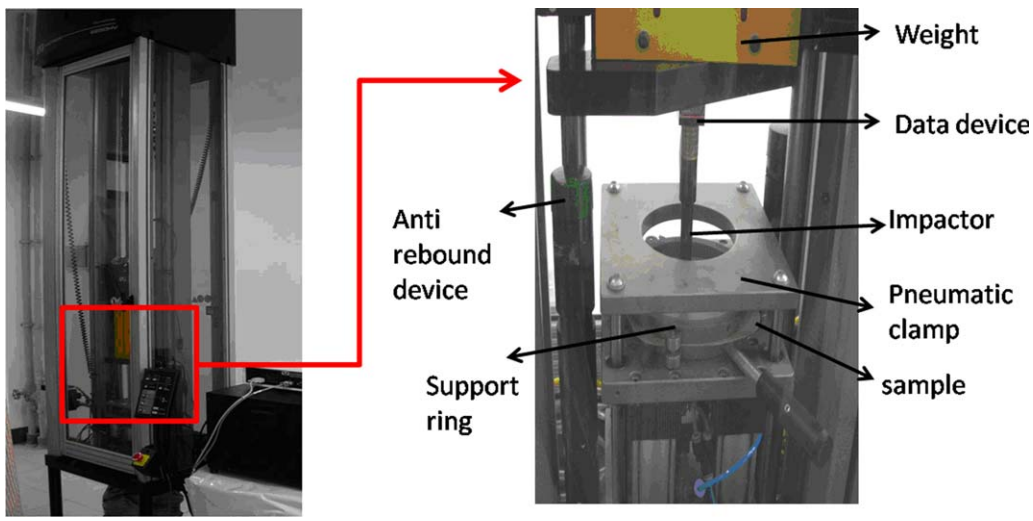

FIG. 4. Instron® testing machine for low-velocity impact test. [Color figure can be viewed in the online issue, which is available at wileyonlinelibrary.com.]

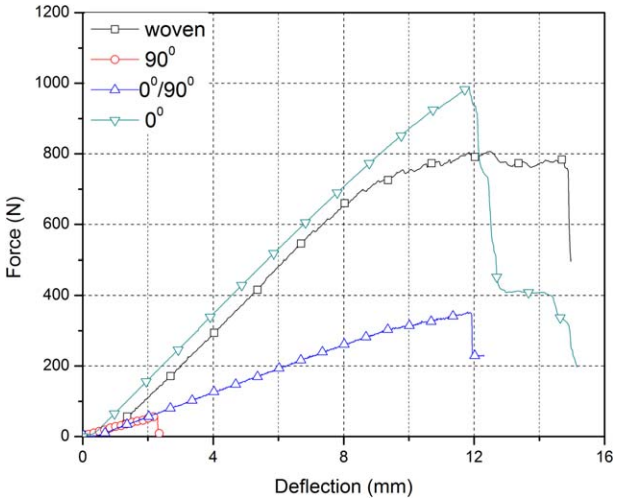

FIG. 5. Force–deflection curve from three-point bending tests. [Color figure can be viewed in the online issue, which is available at wileyonlinelibrary.com.]

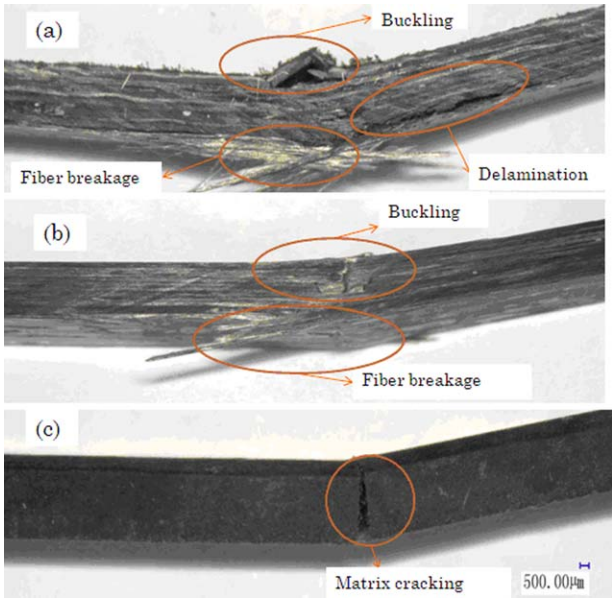

FIG. 6. Damage morphology during three-point bending tests. [Color figure can be viewed in the online issue, which is available at wileyonlinelibrary.com.]

the rate of 2 mm/min. Force (N) and deflection (mm) curves were recorded and the specimens were observed visually to analyze the fracture mode.

Low-Velocity Impact Tests. The low-velocity impact tests were conducted on an Instron® 9250 Drop Weight Impact Testing Machine as shown in Fig. 4. The testing machine was of an antirebound system to prevent multiple impacts on the specimen as shown in Fig. 4. The low-velocity impact tests were performed according to ASTM Standard D 7136 on specimens with dimensions of 140 × 130 × 4 mm^3. The impact tests were carried out by varying the height of the impactor, with fixed mass, to have the required impact energy. The used instrumented impactor was cylindrical in shape with a 12.6 mm diameter hemispherical nose and struck the specimens, simply supported on a ring with a 100 mm internal diameter, in the center, which was pneumatically clamped. Time (ms), energy (J), force (KN), deflection (mm), and velocity (m/s) were recorded and visual inspection was used to determine the type and size of damage area.

RESULTS AND DISCUSSIONS

Three-Point Bending Tests

The force–deflection curves of the three-point bending test results are shown in Fig. 5. It is shown that the bending strength of the 0 sample was the highest of the four samples and 900 laminate was the least. From these curves, it can be shown that under flexural force all the samples failed abruptly except the woven sample which failed in a progressive way. The reason for this type of failure was because of the structure of the woven fabric where the warp yarns and weft yarns were interwoven to form an integrated structure.

Mechanics of materials define bending stress of specimens by the following equation:

$$\sigma = \frac{3FL}{2bh^2} \tag{1}$$

where, σ is the bending stress of the specimen, F is the peak load, L is the span distance, b is the width and h is the thickness. The calculated bending stress of the laminate samples is shown in Table 2.

As expected, the main composite damage modes in the three-point bending test were: resin crack, delamination, and fiber breakage as shown in Fig. 6. For the 90° laminate the damage mode was the resin crack, Fig. 6c, since it was only the resin that was supporting the load. The crack originated from the lower part, which was under tension, while the top part which was under compression did not crack but buckled.

For the other types of laminates, there was buckling on the top part due to compression while fiber breakage

TABLE 2. Peak load and the calculated stress from the three-point bending tests.

Laminate type	Dimensions (mm^3)	Span length (mm)	Peak load (N)	Stress (N/mm^2)	Stress (MPa)
90°	140 × 15 × 4	100	58	36.25	36.25
0°/90°	140 × 15 × 4	100	352	220	220
Woven	140 × 15 × 4	100	780	487.5	487.5
0°	140 × 15 × 4	100	988	617.5	617.5

DOI 10.1002/pc

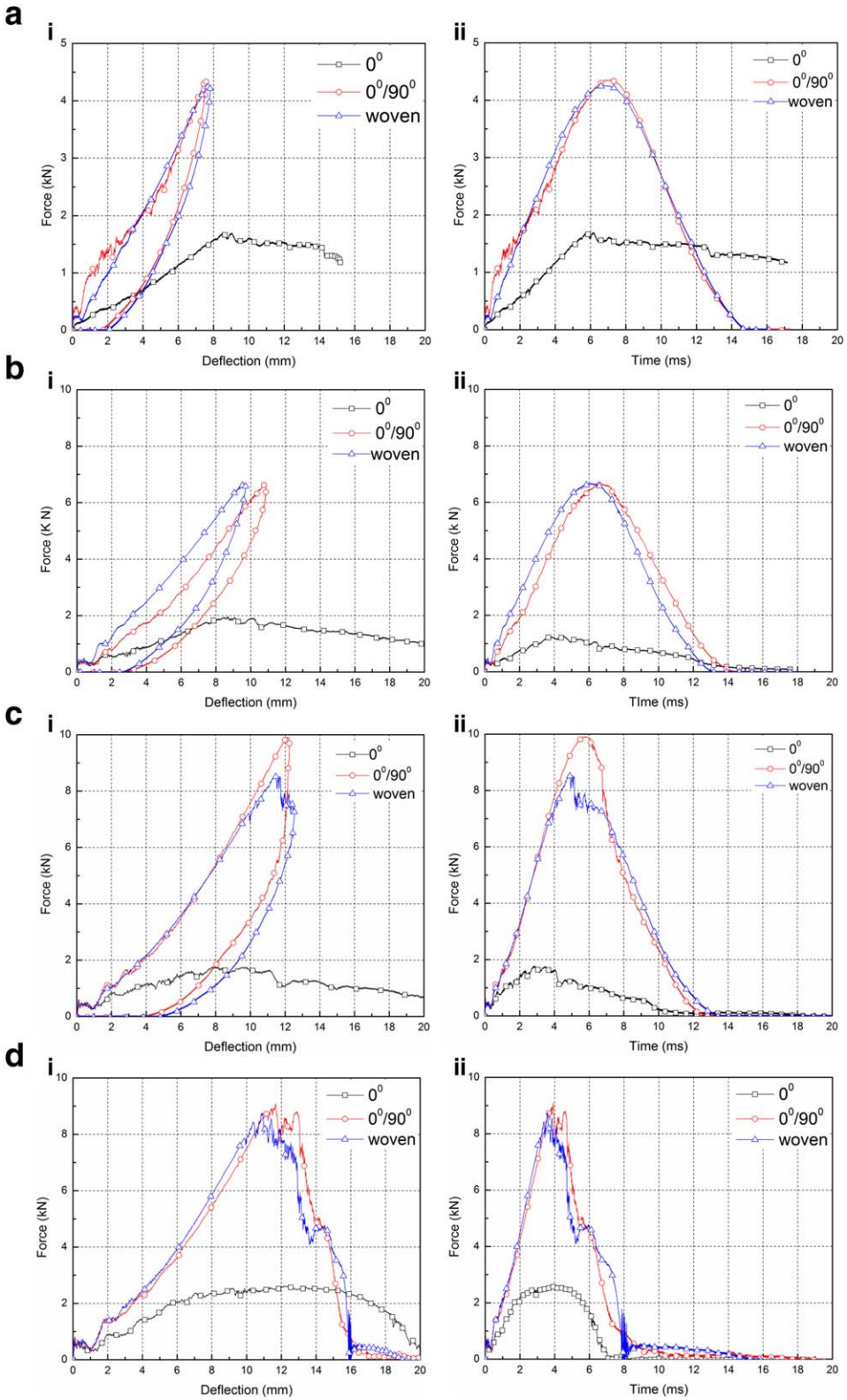

FIG. 7. Comparison of 0, 0/90, and woven laminates under energies of (a) 15, (b) 30, (c) 50, and (d) 70 J using: (i) force–deflection curve and (ii) force–time curve. [Color figure can be viewed in the online issue, which is available at wileyonlinelibrary.com.]

occurred at bottom side due to tension, Fig. 6a and b. Delamination was visible in most laminates within the sample, especially unidirectional and cross-ply laminates. It was noted that when delamination occurred, the load supported by the laminate reduced drastically and the deflection under the load increased.

TABLE 3. Peak loads under different impact energies.

Impact energies (J)	0°	0°/90°	Woven
15	1.70	4.36	4.25
30	1.94	6.61	6.66
50	1.78	9.90	8.52
70	2.62	9.10	8.24

Low-Velocity Impact Testing Results

Force–Deflection Curves. Force–deflection curves under various energies are shown in Fig. 7a (i), b (i), c (i), and d (i). The curves show the capacity of the composite material to react to an impact loading. There are two distinct types of force–deflection curves: closed curve and open curve [20, 21]. Closed type of curves occur at low impact energies and it is characterized by the rebound of the impactor and no or minimal damage to the laminate. This curve shows the elastic response of the laminate upon an impact event. Open type of curve occurs at high impact energies and it is characterized by excessive damage of the laminate composite or complete damage of the composite. It also shows the plastic response of the laminate to an impact event.

The force–deflection curves of cross-ply (0°/90°) and woven laminates were closed curve for energies 15, 30, and 50 J. This showed that the impactor was rebounded and the area under these curves is the energy transferred from the impactor to the laminate and then back to the impactor during rebounds. This was in agreement with the results of Fan et al. [18]. For the 0° laminate, the curves are of the open type showing that there were no rebounds of the impactor at all the energies, but all the energies was absorbed during the impact causing damage to the laminate. The area under the curve refers to the energy absorbed by the laminate during the impact event [20].

From the force–displacement curves and force–time curves, it is evident that the cross-ply (0°/90°) laminates and woven laminates behaved in the same way. Their curves look similar for energies of 15 and 30 J, but at the energies of 50 and 70 J, there is a slightly higher impact force for the cross plies than the woven laminate. This implies that cross-ply had better impact resistance than woven laminates. The similarity in their curves is a subject for further research.

At the beginning of all the impact events, there was an oscillation of the force which took place in the force–deflection curve. This was due to the onset of the damage mechanism which was in agreement with the work of Uyaner et al. [22]. From the force–deflection curve, it can be seen that as the impact energy increased, the impact force as shown in Table 3 and the deflection also increased. From the force–time curve, the time taken to complete the impact event reduced as the impact energy was increased.

The force–deflection curve also shows the damage extent on the laminate during the impact loading event. For 0° laminate, the force–deflection curves are all of the open type, showing that the laminate was damaged in all the energies of 15, 30, 50, and 70 J. The damage of this laminate occurred along the fiber direction because it is only the resin that is holding the fibers in the traverse direction.

For the cross-ply (0°/90°) and woven reinforced laminates, their curves at 15, 30, and 50 J, are all of closed type which is evidence that the laminate was not damaged or there was a small damage. At the higher energy of 70 J, the impactor penetrated the laminates completely destroying them. The force–deflection curve is of the open type as shown in Fig. 7d (i). At the 70 J energy level, deformation energy was reached represented by the area under the force–deflection curve [18], and all this energy was absorbed by the laminate [16].

Force–Time Curves. The force–time graph of the cross-ply and woven laminates are symmetrical in nature for the lower energies of 15 and 30 J as shown in Fig. 7a (ii) and b (ii). The loading time is equal to the unloading time and is symmetrical about the peak load. For higher energies of 50 and 70 J, the curves are different; the loading time is shorter than the unloading time as shown in Fig. 7c (ii) and d (ii). This is clearly seen with the 0° laminates, all of its force–time curves are asymmetrical. The loading time is shorter than the unloading time. This observation can be linked to the damage of the laminate.

Deflection–Time Curves. These curves in Fig. 8, where (i) show the deflection–time curves and (ii) shows velocity time curves at different energies (a. for 15 J, b. for 30 J, c. for 50 J, and d. for 70 J). The deflection–time curve of the 0° laminates shows that damage occurred in all the energies. This is evident by the increasing deflection–time curve. For cross-ply and woven laminates, the deflection–time curve rises to the maximum deflection and falls back to zero showing that there was no damage on the laminate or there was little damage. This occurs in the lower energies of 15, 30, and 50 J as shown in Fig. 8a (i), b (i), and c (i). The deflection of the laminates reaches its maximum value when the load is reaching its maximum value and starts to reduce when unloading occurs [16].

The maximum deflection of the specimen is governed by the impact energy. The deflection of the laminate during an impact event is mainly due to the laminate stiffness. Before the laminate is damaged, deflection occurs when the impactor strikes it because of its stiffness. In examining the deflection, it was noted that it was always twice the size of the plate thickness for both the cross-ply and woven laminates [17]. The deflection–time curves of cross-ply and woven laminates for the lower energies of 15, 30, and 50 J, behave in the same way and follows the same pattern as shown in Fig. 8a (i), b (i), and c (i). They rise to the maximum value and falls to zero at the end of the impact event. At the higher energy of 70 J, the deflection–

 DOI 10.1002/pc

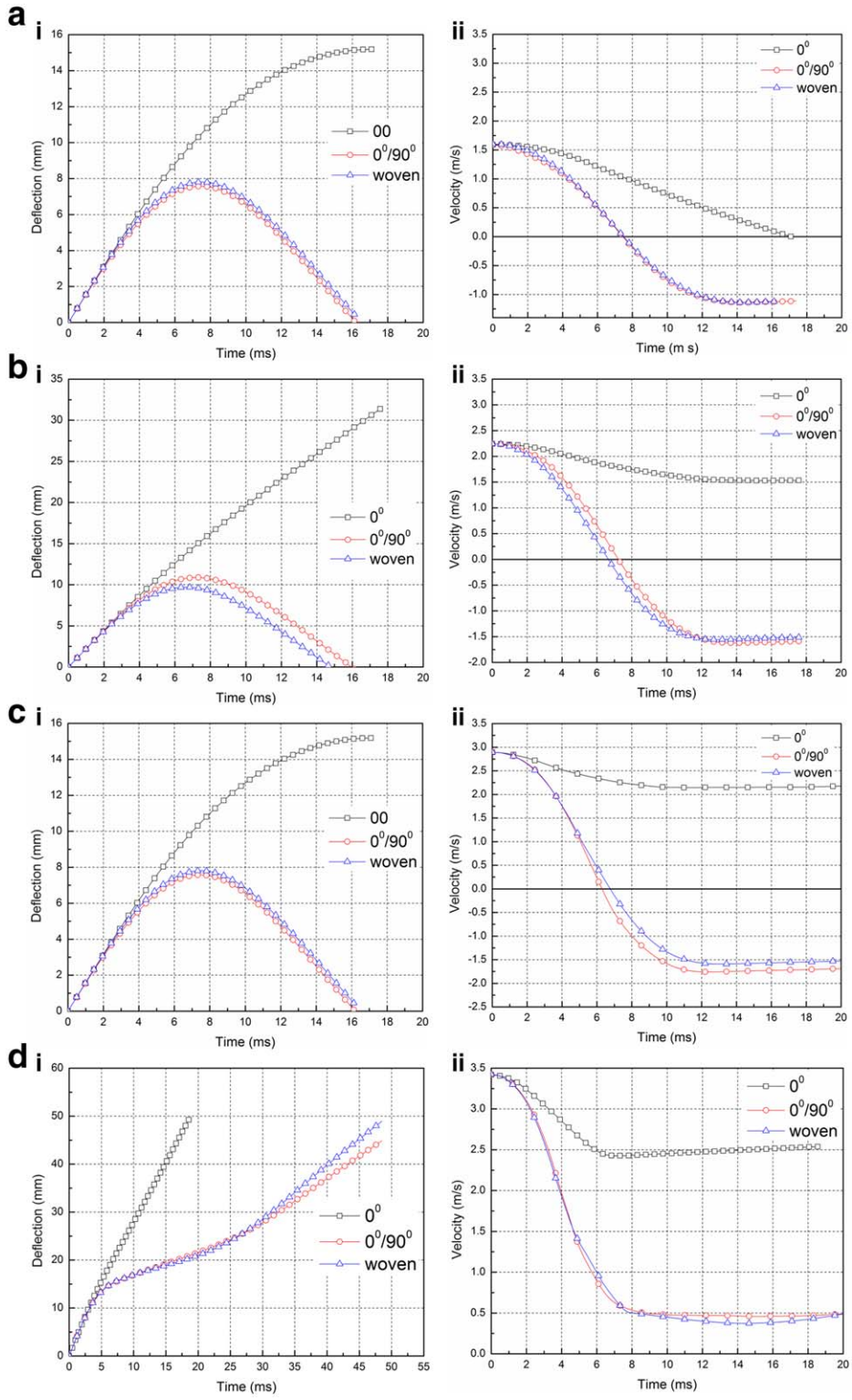

FIG. 8. Comparison of 0, 0/90, and woven laminates under energies of (a) 15, (b) 30, (c) 50, and (d) 70 J using: (i) deflection–time curves and (ii) velocity–time curves. [Color figure can be viewed in the online issue, which is available at wileyonlinelibrary.com.]

time curve of the cross-ply (0°/90°) and woven laminates continuously increases and does not return to zero showing that the laminates were damaged at this energy [Fig. 8d (i)].

Velocity–Time Curves. The velocity–time curve for the 0° laminate falls from a higher value to zero for the energy of 15 J, showing that the impactor was brought to rest by the laminate, Fig. 8a (ii). For the higher energies

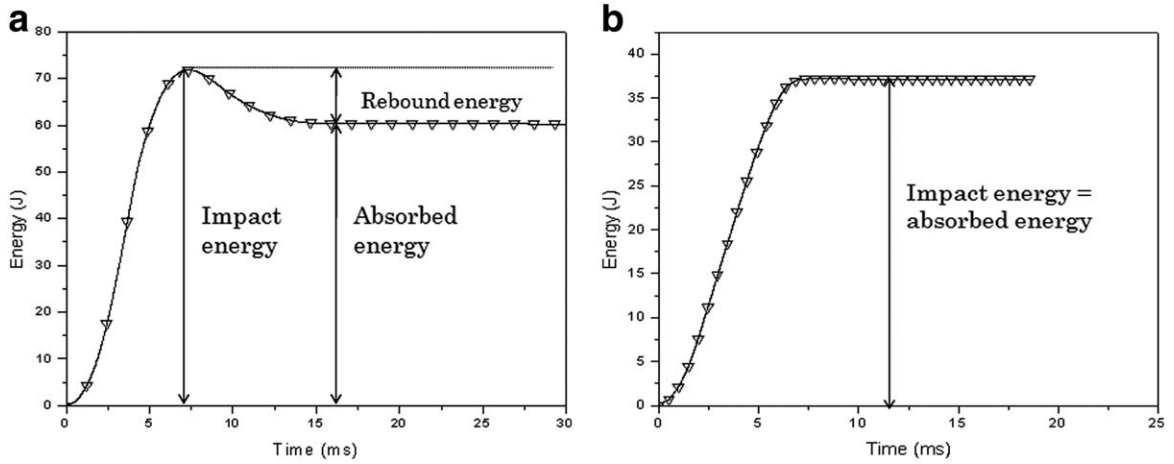

FIG. 9. Energy–time curves for an impact event. (a) Rebound case and (b) nonrebound case.

of 30, 50, and 70 J, the velocity time curve for the 0° laminate falls from the higher value to a lower constant value, but not to zero, this shows that the impactor perforated the laminate and exited on the other side of the laminate with the constant value, Fig. 8b (ii), c (ii), and d (ii). The difference in the initial higher value of velocity and the lower constant value gives the lost kinetic energy by the impactor due to the energy absorbed by the

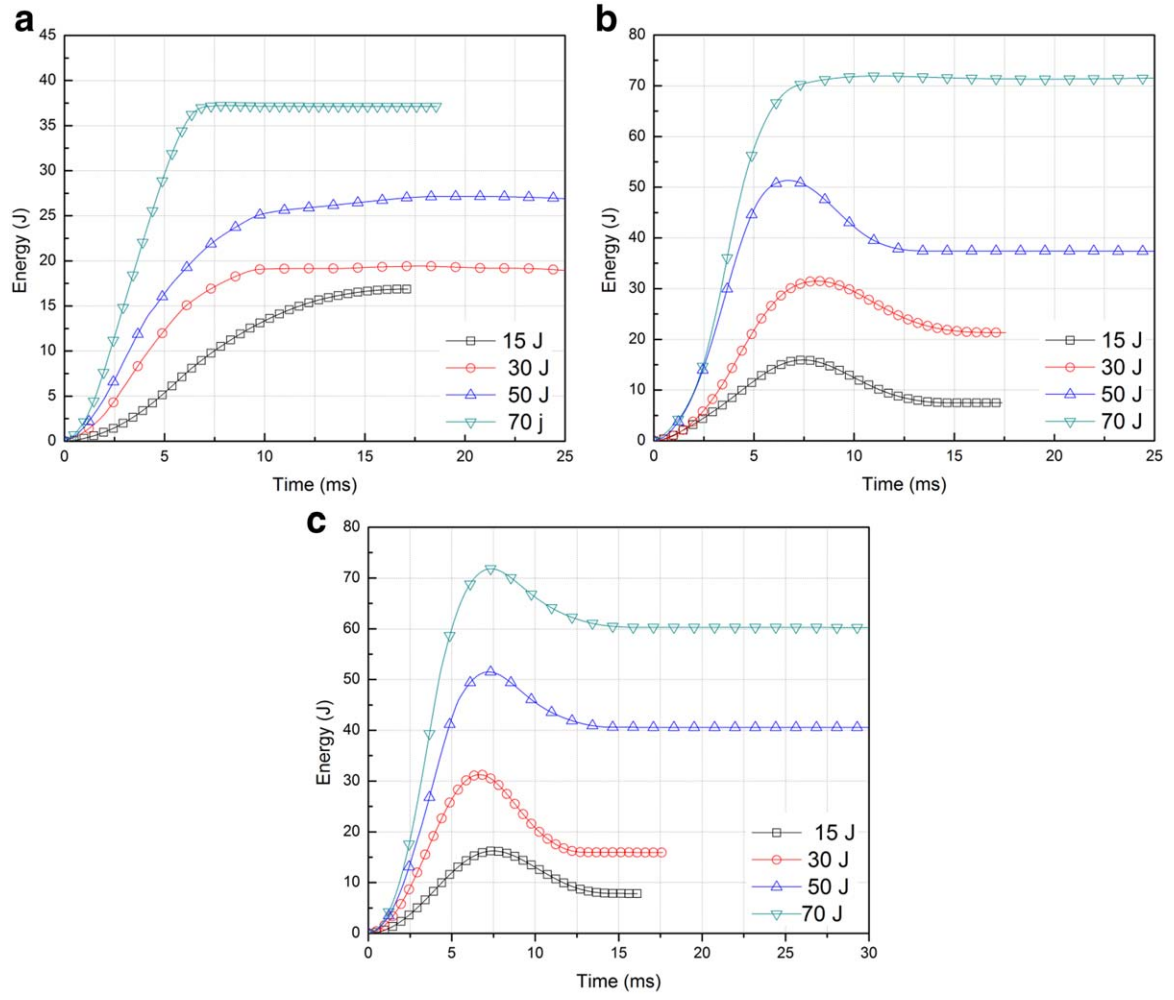

FIG. 10. Energy–time curves for laminates (a) 0 laminates, (b) 0/90 laminates, and (c) woven laminates. [Color figure can be viewed in the online issue, which is available at wileyonlinelibrary.com.]

 DOI 10.1002/pc

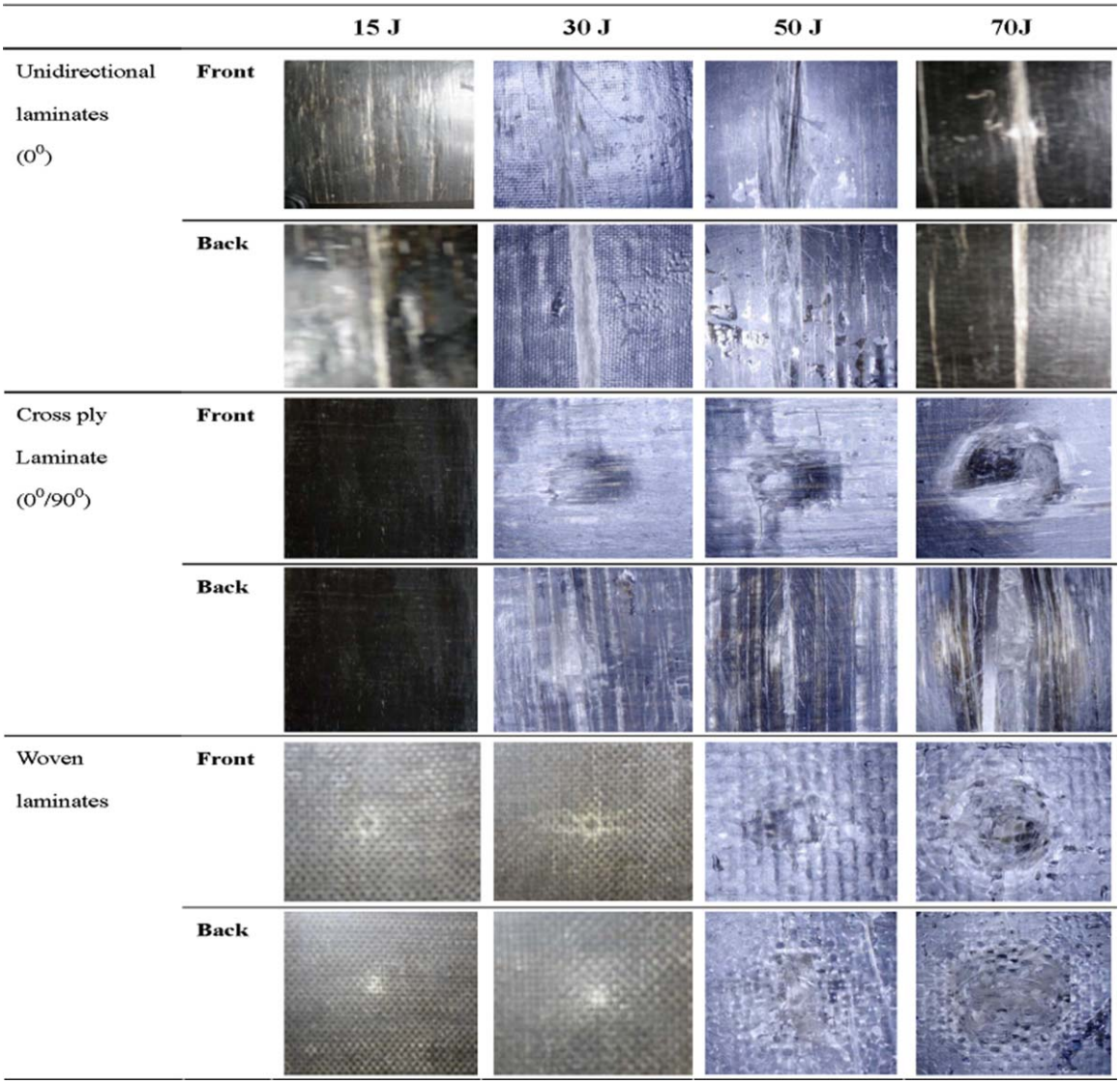

FIG. 11. Damage morphologies. [Color figure can be viewed in the online issue, which is available at wileyonlinelibrary.com.]

laminate. The absorbed energy was responsible for the damage of the laminate.

The velocity–time curves of the cross-ply and woven laminates behaves in the same, but different from the 0° laminate. For the lower energies of 15, 30, and 50 J, Fig. 8a (ii), b (ii), and c (ii), the velocity of the impactor reduces from the higher value and reaches zero at the same time when load is reaching its maximum value. It changes direction and increases to the negative side showing that it rebounds from the laminate [23]. The higher negative velocity value reached by the impactor was lower than the corresponding initial positive value. This was because not all the energy given to the laminate by the impactor was given back to the impactor; the difference damaged the laminate. At higher energy of 70 J, the velocity–time curve does not fall to zero, but it reduces to a lower constant value, Fig. 8d (ii). This shows that the laminate was damaged and the impactor exited the laminated on the back side with a lower constant velocity. The difference in the exiting velocity and the initial velocity gives the energy absorbed by the laminate. This energy damages the laminate and it affects the failure modes during the impact event.

Energy–Time Curves. The impact energy (E_i) is the total sum of energy transferred from the impactor to the composite laminate. It is the same as the kinetic energy possessed by the impactor just before it strikes the laminate. The absorbed energy (E_a) is the energy absorbed by the composite laminate in form of damage and friction between the impactor and the composite laminate [21]. There are two types of energy–time curves: one where rebound occurs and the other where rebound does not occur as shown in Fig. 9.

The energy transferred from the impactor to the laminate increased with the impact energies. At higher impact energy, the laminate absorbed a lot of energy by breaking. The energy increased with time and reached a maximum value at the same time when the contact force reached the peak value. The curve decreased and finally reached a constant value, which was the energy absorbed by the laminate. The maximum value of each curve represented the associated peak impact force. The difference between the two energies was retained in the impactor and used to rebound the impactor [21]. The 0° laminates absorbed all the energy as evidence by the time–energy curve as shown in Fig. 10a. Cross-ply (0°/90°) and woven laminates absorbed part of the energy in the lower energies of 15, 30, and 50 J and the remainder was retained in the impactor which was rebounded upon impact, Fig. 10b and c. At higher energy of 70 J, the impactor rebounded from woven laminate but not from cross-ply (0°/90°). This showed that at this energy, cross-ply laminate absorbed more energy than woven laminate through excessive damage.

The laminate absorbs energy in two different ways: being elastic and rebounding the impactor, and being plastic and through damage. The main damages that occurred were resin crack, delamination, and fiber breakage. It was observed that the major energy absorption mechanism of basalt fiber reinforced laminates was fiber breakage mode [20, 24–26].

Damage Morphologies. The main damage mode of unidirectional (0°) laminate was resin crack. The laminate broke along the fiber for all the energies as shown in Fig. 11. This happened because only resin was holding the fibers along the transverse direction. For cross-ply and woven laminates, damage was not clearly visible at the lower energy of 15 J, it started to appear at the energy of 30 J, inform of a small indentation in the impacted side and fiber bending in the nonimpacted side in both laminates.

At the energy of 50 J, resin crack was visible on the impacted side leading to a deeper indentation and fiber breakage on the non impacted side due to excessive bending of fibers. This was in agreement with the work of Evci et al. [26]. At the higher energy of 70 J, both the cross-ply and the woven laminates were perforated by the impactor. The visible damage shape on the impacted side in cross-ply and woven laminates was circular as shown in Fig. 11. The diameter of the circular damaged area was the same as that of the impactor. The back side showed complete fiber breakage in woven laminates and in cross-ply it was fiber breakage plus excessive delamination in the direction of fibers of the last lamina.

CONCLUSIONS

The behavior of basalt unsaturated polyester laminates when subjected to static three-point bending loading and low-velocity impact loading were studied. Three stacking sequences studied were unidirectional (0°), cross-ply (0°/90°) and woven laminates. Converse to the impact loading response, the maximum load bearing capacity and strength of unidirectional composite (0° laminate) was found to be higher than those of plain woven and cross-ply laminates under static three-bending loading. It was then concluded that unidirectional (0°) laminate is superior to the woven and cross-ply in static loading while cross-ply (0°/90°) and woven laminates are superior in dynamic loading, respectively.

The loading events showed that the response of laminate systems depends on the elastic properties of the fiber material and the stacking sequence used. The force–displacement, force–time, deflection–time, velocity–time, and energy–time curves for each case have been drawn and used to compare the three stacking sequences. Basalt unsaturated polyester laminates response to impact loading either in elastic way at lower energy or plastic way at higher energy. The basalt unsaturated polyester laminates exhibited four types of failures: resin crack, delamination, fiber breakage, and perforation. It was concluded that the major energy absorption mechanism in basalt unsaturated polyester reinforced laminate was fiber breakage.

ACKNOWLEDGMENTS

The authors acknowledge the financial supports from the National Science Foundation of China (Grant Number 11272087). The financial supports from Foundation for the Author of National Excellent Doctoral Dissertation of PR China (FANEDD, No. 201056) and the Fundamental Research Funds for the Central Universities of China are also gratefully acknowledged.

REFERENCES

1. Q. Liu, M.T. Shaw, R.S. Parnas, and A.M. McDonnell, *Polym. Compos.*, **27**, 41 (2006).
2. B. Wei, H. Cao, *and S. Song, Mater. Des.*, **31**, 4244 (2010).
3. V. Manikandan, J.T.W. Jappes, S.M.S. Kumar, and P. Amuthakkannan, *Compos. Pt. B Eng.*, **43**, 812 (2012).
4. I. Mokhtar, M.Y. Yahya, M.R.A. Kadir and M.F. Kambali, *Polym. Plast. Technol. Eng.*, **52**, 1140 (2013).
5. T. Deak and T. Czigany, *Text. Res. J.*, **79**, 645 (2009).
6. V. Lopresto, C. Leone, and I.D. Iorio, *Compos. Pt. B Eng.*, **42**, 717 (2011).
7. R.J. Varley, W. Tian, K.H. Leong, A.Y. Leong, F. Fredo and M. Quaresimin, *Polym. Compos.*, **34**, 320 (2013).
8. T. Czigány, *Compos. Sci. Technol.*, **66**, 3210 (2006).
9. J. Militký, V. Kovacic, and V. Bajzík, *Fibres Text. East. Eur.*, **15**, 64 (2007).
10. X. Wang, B. Hu, Y. Feng, F. Liang, J. Mo, J. Xiong, and Y. Qiu, *Compos. Sci. Technol.*, **68**, 444 (2008).
11. M.T. Dehkordi, H. Nosraty, M.M. Shokrieh, G. Minak, and D. Ghelli, *Mater. Des.*, **31**, 3835 (2010).

12. S.M.R. Khalili, V. Daghigh, and R.E. Farsani, *J. Reinf. Plast. Compos.*, **30**, 647 (2011).
13. S. Carmisciano, I.M.D. Rosa, F. Sarasini, A. Tamburrano, and M. Valente, *Mater. Des.*, **32**, 337 (2011).
14. C. Colombo, L. Vergani and M. Burman, *Compos. Struct.*, **94**, 1165 (2012).
15. K.H. Tan and Y.Q. Zhou, *J. Compos. Constr.*, **15**, 304 (2011).
16. N.R. Mathivanan and J. Jerald, *Mater. Des.*, **31**, 4553 (2010).
17. M. Aktas, C. Atas, B.M. Icten, and R. Karakuzu, *Compos. Struct.*, **87**, 307 (2009).
18. J.Y. Fan, Z.W. Guan, and W.J. Cantwell, *Polym. Compos.*, **32**, 1380 (2011).
19. N.V. Padaki, R. Alagirusamy, B.L. Deopura, B.S. Sugun and R. Fangueiro, *Indian J. Fibre Text. Tes.*, **33**, 189 (2008).
20. C. Atas and O. Sayman, *Compos. Struct.*, **82**, 336 (2008).
21. C. Atas, Y. Akgun, O. Dagdelen, B.M. Icten and M. Sarikanat, *Compos. Struct.*, **93**, 1178 (2011).
22. M. Uyaner and M. Kara, *J. Compos Mater.*, **41**, 2877 (2007).
23. E.M. Soliman, M.P. Sheyka and M.R. Taha, *Int. J. Impact Eng.*, **47**, 39 (2012).
24. G. Belingardi and R. Vadori, *Int. J. Impact Eng.*, **27**, 213 (2001).
25. N.F. Rilo and L.M.S. Ferreira, *Int. J. Mech. Mater. Des.*, **4**, 291 (2008).
26. C. Evci and M. Gulgec, *Int. J. Impact Eng.*, **43**, 40 (2012).